

# Examination of the Flame Transmission Through Porous Structures

S. MECKE<sup>1</sup>, D. MARKUS<sup>1,\*</sup>, C. SCHOLZ<sup>1</sup>, M. THEDENS<sup>1</sup>, H. D. KIM<sup>2</sup>, F. ENGELMANN<sup>3</sup>,  
A. HILLIGER<sup>3</sup> AND U. KLAUSMEYER<sup>1</sup>

<sup>1</sup>*Department 3.5 Flame Transmission Processes, Physikalisch-Technische Bundesanstalt, Braunschweig, Germany*

<sup>2</sup>*Center for Safety Testing and Certification, Korea Occupational Safety & Health Agency, Incheon, Korea*

<sup>3</sup>*KEK GmbH, Bad Schmiedeberg, Germany*

Porous structures can be used to avoid flame transmissions as it is done in flame arresters or breathing devices of explosion protected equipment. A detailed examination of the different flame transmission behaviours of different porous structures is performed using several methods of laser diagnostics. The flow behaviour is analysed using a Schlieren technique and the flame transmission itself is examined using laser induced fluorescence of OH radicals.

*Keywords:* Flame arresters, flame transmission, quenching, porous structure, OH LIF, explosion.

## INTRODUCTION

In chemical facilities and other industrial areas explosive atmospheres can occur. In these locations numerous tasks to either avoid explosions or at least to reduce the consequences to a non-hazardous measure are done. An important technical component used for this protection method is the mechanical flame arrester element. Flame arrester elements allow mass transport by gas flow on the one hand and on the other hand they avoid flame transmission. That is to say they are able to uncouple volumes concerning explosions and flames but still enabling gas exchange between them.

The two main fields of application of flame arrester elements are breathing devices and flame arresters. Breathing devices are for example an important part of gas sensors for use in explosive atmospheres. These gas sensors are often designed in type of protection “flameproof enclosure” which allows the electronic measuring equipment of the gas sensor to generate high temperatures for instance. These temperatures are needed for the function of some measuring principles. The aim of the flameproof enclosure is to avoid an explosion that may occur inside the enclosure from igniting the surroundings. It is necessary for the functioning of the gas sensor to ensure a gas exchange

---

\*Corresponding author: Detlef.Markus@ptb.de

between the electronic measuring equipment of the sensor and the surroundings via a breathing device. The main requirements for this breathing device are on the one hand to enable transportation by diffusion of gas or vapour as fast as possible and on the other hand to avoid flame transmission from the inner side of the sensor to the surroundings. Another field of application for flame arrester elements is the use in flame arresters which are used to uncouple different parts of chemical facilities concerning explosions and flames. The requirements with respect to the function of this flame arrester elements are similar to those used as breathing devices, namely to avoid flame transmissions and to commit a pressure loss as low as possible while being passed through by a fluid. With the difference that the transport mechanism in the case of flame arresters is not diffusion but a forced flow.

In this paper a new porous material is examined concerning its properties for the use as a flame arrester element and it is compared with traditional flame arrester elements made of crimped ribbon. The comparison of the different flame arrester elements is based on the flame transmission behaviour measured by a safe gap as well as the examination of the hot gas flow leaving the flame arrester element by Schlieren technique and laser induced fluorescence of OH radicals.

The safe gap can be determined by a testing apparatus similar to the MESG testing apparatus (IEC 60079-1-1 [2002]) which was developed to characterise porous materials for the use as flame arrester elements (Mecke *et al.* [in press]). This apparatus uses H<sub>2</sub>/air mixtures characterised with the MESG testing apparatus concerning the dependency of the safe gap from initial pressure for the analysis of porous structures. With the help of the determination of a safe initial pressure at which a flame propagation through the porous structure just fails to occur, a safe gap can be attached to every porous structure. Using this safe gap value as a measure for the property of a porous structure to avoid flame transmission, it is possible to put the structures in an order concerning their flame quenching qualities.

Every flame arrester leads to a pressure loss that requires pump capacity and therefore higher power consumption. So in most cases it is not only essential

for flame arresters to prevent a flame transmission in all situations they are certified for but also to be optimized concerning flow resistance. The task of a pipeline for example is the transportation of gas whereas the flame arrester has to ensure the safety of the industrial area without disturbing the transportation more than absolutely necessary. Therefore, a comparison of the flow resistance properties of flame arrester elements is done in addition to the flame transmission examinations.

## THEORY

The transmission of a gas explosion through porous structures is an instationary and spatially inhomogeneous process strongly influenced by turbulence and chemical reactions. The technique of laser induced fluorescence (LIF) gives spatially and temporally resolved information and has been successfully used in highly turbulent environments due to its high sensitivity and species specificity with high spatial and temporal resolution (Eckbreth [1996]). One intermediate species that is produced in the reaction zone during ignition process is OH. Therefore OH radicals can be used as an indicator for the reaction zone. The radicals can be detected by measuring the fluorescence that follows their excitation by a laser. This paper presents the results obtained using simultaneously OH-LIF and laser Schlieren imaging of the transmission of gas explosions through porous structures. The OH-LIF images were used to examine the ignition processes inside the hot gas flow and the laser Schlieren images were used in studying the temporal development of the flow.

The transportation of fluids through porous media by forced flow, like occurring in flame arresters during normal operation (without any explosions) can involve several simultaneously occurring mechanisms. If the pore size of the porous structure is big compared to the mean free path of the gas molecules the following equation can be used. It includes only the mechanisms of viscous and inertia flow following Schatt *et al.* [2007]

$$\Delta p = \frac{\dot{V} \cdot s}{A} \left( \frac{\eta}{\alpha} + \frac{\rho \cdot \dot{V}}{A \cdot \beta} \right). \quad (1)$$

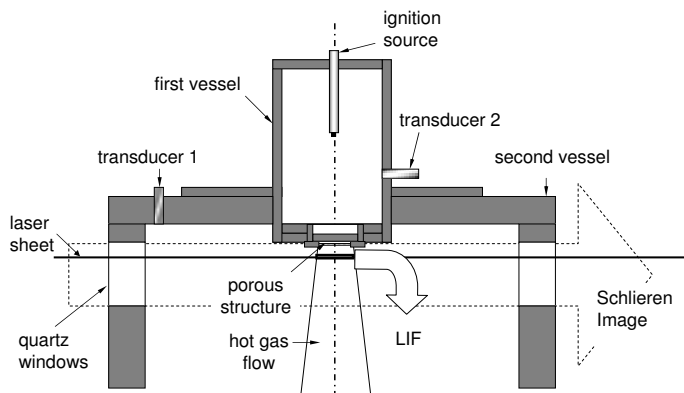


FIGURE 1  
Schematic of combustion vessel.

In this equation  $\Delta p$  is the pressure loss over the porous structure induced by a constant volume flow  $\dot{V}$ . The dynamic viscosity  $\eta$  and the density  $\rho$  are describing the fluid. The porous structure has got the thickness  $s$  and the surface area  $A$  perpendicular to the direction of the flow. The symbols  $\alpha$  and  $\beta$  are the viscous and inertia permeability coefficients, respectively. In the case of the laminar flow there is loss resulting from friction between fluid and walls. The loss of energy in the inertia flow consists of the change of flow direction and the resulting turbulences during the flow through the wounding pores. In this paper Eq. (1) shall be used to clarify the interrelationship between kind and geometry of a flame arrester element and its flow behaviour. Therefore it is reasonable to convert Eq. (1) to the following form:

$$\Delta p = \frac{s \cdot \eta}{A \cdot \alpha} \cdot \dot{V} + \frac{s \cdot \rho}{A^2 \cdot \beta} \cdot \dot{V}^2 = B \cdot \dot{V} + C \cdot \dot{V}^2. \quad (2)$$

The factors  $B$  and  $C$  in Eq. (2) shall be deemed to be constant for a specific porous structure to simplify the consideration of the flow behaviour. In Eq. (2) the composition of viscous and inertia flow is easily visible. The permeability coefficients  $\alpha$  and  $\beta$  can be experimentally determined concerning ISO 4022 [2006].

## EXPERIMENTAL SETUP

An experimental set-up, well defined and optically accessible, is used for the current studies consisting of

a combustion vessel as shown in Figure 1 (Sadanandan *et al.* [2007]). The test porous structure which has to be analysed is fixed between two vessels. Vessel 1 is 80 mm in length and 60 mm in diameter leading to a volume of 0.226 litres. This vessel is flanged to vessel 2, which has a volume of 12 litres. It is provided with three quartz windows for optical access. Both the vessels are filled with 27.5% hydrogen/air mixtures at the beginning of each experiment. The fuel/air mixture in vessel 1 is ignited by means of electrical discharges on the symmetrical axis of the vessel at a distance of 56 mm from the outer face of the porous structure. The pressure rise in both the vessels is recorded by means of Kistler (Model 6031) transducers. The hot burned gases expand into vessel 2 through the porous structure. The development of the hot gas flow using the Schlieren technique is captured perpendicular to the flow by means of an ICCD camera. The laser sheet used to excite OH radicals inside the hot gas flow crosses vessel 2 parallel to the porous structure. The subsequent fluorescence is collected perpendicular to the laser sheet through a window in the bottom of vessel 2 using a second ICCD camera.

The exciting laser pulses for OH-LIF were obtained using the frequency doubled output from a dye laser (Rhodamine 6G) pumped by a frequency doubled (532 nm) Nd:YAG laser (Figure 2). The dye laser was tuned to the  $Q_1(5)$  transition at 283 nm in the  $v'' = 0, v' = 1$  band of the  $A^2\Sigma^+ - X^2\Pi$  system. The laser beam was formed into a sheet of approximately

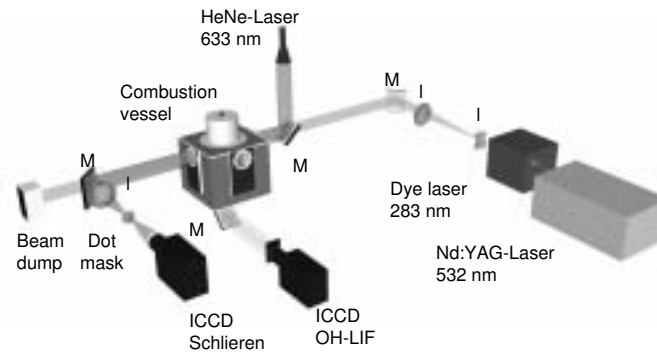


FIGURE 2  
Schematic of optical setup used for simultaneous Schlieren and OH-LIF (M: mirror, I: lens).

30 mm in width and 0.2 mm in thickness by means of cylindrical lenses. Subsequent fluorescence from the OH radical was observed using a UG11 filter in front of the camera lens which also eliminates nearly all reflections of laser light. For the LIF visualization a Flame Star high speed ICCD camera (La Vision, 12 bit,  $384 \times 288$  pixel array) coupled to an UV lens (Halle, 100 mm,  $f/2$ ) was used.

The laser Schlieren optical system consists of a He-Ne laser (20 mW,  $\lambda = 632.8$  nm) as a point source, a beam expander for collimating the beam and a subsequent lens-knife edge combination to obtain the Schlieren image. For the laser Schlieren imaging a high speed ICCD camera (La Vision Streak Star, 14 bit,  $384 \times 550$  pixel array) coupled to a Sigma zoom lens (75-300, 4-5.6 f) was used. Sequential Schlieren images were taken during each experiment with time steps between  $50 \mu\text{s}$  up to  $200 \mu\text{s}$  and  $1 \mu\text{s}$  exposure time. The timing between ignition, laser pulse and the different camera gate openings were adjusted by means of a delay generator circuit.

## RESULTS

The safe gaps according to Mecke *et al.* [in press] were determined for several test samples. The test samples consist of a new material called fibre structure as well as of classical crimped ribbon flame arrester elements. The new material is a kind of powder metallurgically manufactured sintered metal. The basic

material, in contrast to conventional sintered metals, consists in short metallic fibres instead of metallic powder. Due to the stretched geometry of the fibres it is possible to create porous structures up to a porosity of 95%, which still have good mechanical stability (Steigert *et al.* [2000]).

In Table 1 the safe gap and some specifications of a few test samples are shown. The Fibre structures (called fibre in Table 1) are specified by their porosity  $\varepsilon$ , which is defined as

$$\varepsilon = \frac{\rho_{\text{solid}} - \rho_{\text{porous structure}}}{\rho_{\text{solid}}} \cdot 100\% \quad (3)$$

and the thickness of the test sample  $t_t$  as well as the average length  $l_f$  and diameter  $d_f$  of the fibres. The crimped ribbon structures (called ribbon in Table 1) are specified by their width of gap  $w_g$  (that is the height of the triangle formed by the ribbon), the thickness of the ribbon  $t_r$  and the overall thickness of the test sample  $t_t$ . With the help of the safe gap it is possible to sort the samples according to their resistance against flame transmission as done in Table 1. The safe gap value is a measure for the property of porous structures to avoid flame transmission but it gives no information concerning the flame transmission itself. Therefore the examination of the hot gas flow using Schlieren technique and laser induced fluorescence of OH radicals was done. Figure 3 shows Schlieren series for two test samples (No. 2 and No. 5, Table 1). Each image shows the region from 5 mm to 33 mm beneath the test sample in vessel 2 (Figure 1)

TABLE 1

Specification of test samples;  $l_f$  means length of fibre,  $d_f$  diameter of fibre;  $w_g$  width of gap,  $t_r$  thickness of ribbon,  $\varepsilon$  porosity and  $t_t$  thickness of test sample; all (including safe gap) in mm.

No.	Kind	Specification	Safe gap
1	Fibre	$l_f = 13$ ; $d_f = 0.07$ ; $\varepsilon = 61$ ; $t_t = 1.0$	<0.15
2	Ribbon	$w_g = 0.15$ ; $t_r = 0.15$ ; $t_t = 10.0$	<0.15
3	Fibre	$l_f = 13$ ; $d_f = 0.1$ ; $\varepsilon = 78$ ; $t_t = 3.0$	0.16
4	Fibre	$l_f = 13$ ; $d_f = 0.1$ ; $\varepsilon = 85$ ; $t_t = 4.2$	0.29
5	Ribbon	$w_g = 0.3$ ; $t_r = 0.15$ ; $t_t = 10.0$	0.33
6	Fibre	$l_f = 20$ ; $d_f = 0.2$ ; $\varepsilon = 79$ ; $t_t = 5.0$	0.33
7	Fibre	$l_f = 20$ ; $d_f = 0.15$ ; $\varepsilon = 82$ ; $t_t = 5.0$	0.34
8	Fibre	$l_f = 13$ ; $d_f = 0.1$ ; $\varepsilon = 88$ ; $t_t = 2.8$	0.43
9	Fibre	$l_f = 20$ ; $d_f = 0.25$ ; $\varepsilon = 78$ ; $t_t = 4.8$	0.44

in which the hot gas flows from top to bottom. The experiments were performed using 27.5 vol.% H<sub>2</sub> in air at  $p = 1$  bar. In Figure 3(a) the Schlieren series starts 2500  $\mu$ s after the ignition in vessel 1 with  $\Delta t = 100$   $\mu$ s between each image. In this experiment test sample No. 2 is used and no flame transmission occurs.

Figure 3(b) shows a Schlieren series with  $\Delta t = 50$   $\mu$ s between each image using the porous structure No. 5 starting 1950  $\mu$ s after the ignition. In this experiment flame transmission can be observed. These series show two main differences. First, the hot gas in Figure 3(a) enters vessel 2 later than in Figure 3(b) due to the higher flow resistance of the test sample No. 2 compared to No. 5. Second the velocity of propagation of the boundary between hot and cold gas is much faster in the Schlieren images shown in Figure 3(b) due to the acceleration caused by the initiated explosion in vessel 2.

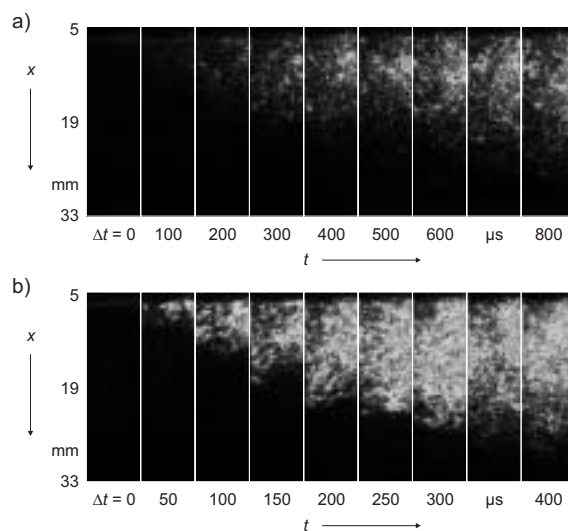


FIGURE 3 Schlieren series a) without flame transmission (test sample No. 2, 2500  $\mu$ s after ignition), b) with flame transmission (test sample No. 5, 1950  $\mu$ s after ignition) (27.5% H<sub>2</sub> in air,  $p = 1$  bar).

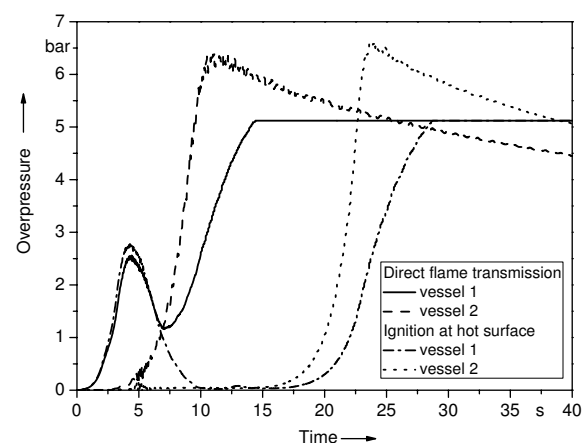


FIGURE 4 Pressure histories of direct flame transmission and ignition at the hot surface of a porous structure.

Figure 4 shows the pressure history of two different experiments done with two samples of the same kind (sample No. 9, Table 1). To get more meaningful results the experiments were done with several test samples with identical specifications. For each experiment there are two pressure curves, measured by the pressure sensors in vessel 1 and in vessel 2, respectively. The

pressure curves of the sensor located in vessel 1 show two maxima. The signal of the second maximum is cut off at 5 bar to get a better resolution of the displaying device. The first pressure maximum displays the explosion in vessel 1 which is decompressed by the porous structure. The second maximum results of an explosion in vessel 2 that is ignited by the flame propagation through the tested flame arrester element. As visible in Figure 4 there is a big discrepancy between the pressure histories of the two experiments. In the first experiment the pressure rise in vessel 2 starts at the moment the pressure in vessel 1 reaches its maximum (about 4 ms after the ignition). That means that there is a direct flame transmission through the sample which occurs when the flame in the forced hot flow, driven by the explosion pressure, is not quenched in the porous structure. The experiment with test sample No. 5 generates a very similar pressure history.

The second experiment shows a much greater span of time between ignition in vessel 1 and in vessel 2. The pressure rise in vessel 2 starts about 15 ms after the ignition in vessel 1. Therefore it is obvious that the explosion in vessel 2 does not result of a direct flame propagation. The igniting process can be described in the following way: Due to the rising pressure after the ignition a forced flow through the sample is developing. In the first phase of this flow cold unburned gas/air mixture passes the porous structure. When the flame front arrives at the inner face of the sample, the combustion is forced to take place into the porous structure. So the combustion zone gets divided into many parts all surrounded by cold walls. Therefore a heat exchange between the chemical reaction and the walls occurs. In this experiment the combustion was stopped by the loss of heat, so that no direct flame transmission could occur. Until the pressure in both chambers has equalised hot exhaust gas is flowing through the porous structure. This leads to a surface temperature of the structure on the outer side which is high enough to ignite the gas/air mixture in vessel 2. The long time between the end of the forced flow (pressure has equalised) and the ignition on the hot surface results in the fact that the "fresh" gas-air mixture was displaced from the hot surface by the exhaust gas and therefore has to get in contact with the ignition source first. This

ignition on the hot surface of a porous structure is a phenomenon settled between direct flame transmission and no ignition in vessel 2. It does not occur at every porous structure with nearly the same specifications because of very small differences in the maximum pore size for instance can result in a changed behaviour.

With the help of the Schlieren series (Figure 3) and the pressure history (Figure 4) it is possible to roughly predict where and when the ignition in vessel 2 occurs. In the case of a direct flame transmission the ignition in vessel 2 occurs before the pressure rise in this vessel gets measurable (earlier than 4 ms after the ignition in vessel 1). The ignition is located just beneath the test sample which is visible from Figure 3(b) because of the constancy in the hot gas flow. According to this information it is reasonable to place the laser sheet for the OH-LIF images as close as possible to the porous structure to watch the ignition in vessel 2. Due to reflections of the laser light at the porous structure itself and its retaining ring, 13 mm between the test sample and the laser sheet is the best distance. Figure 5 shows four OH-LIF images with simultaneously taken Schlieren exposures. The left column of Figure 5 shows the time after ignition in vessel 1 when the images were taken. The column in the middle shows the OH-LIF images.  $I_{LIF}$  is the intensity of excited OH radicals with an arbitrary unit (a.u.) with bright areas standing for more and dark areas for less OH radicals. The intensity of the image is depending on the used amplification. The white circle with the dot in its center, drawn at the OH-LIF image, symbolizes the geometry of the crimped ribbon flame arrester element used in these experiments. The bright shine on the middle axis of the picture just outside the circle consists of reflection on the retaining ring. The right column shows Schlieren images taken at the same time as the OH-LIF images to illustrate the dependency between hot gas flow and combustion reaction. The 13 mm line in the Schlieren image shows where the laser sheet for the OH-LIF analysis is located. It is possible to start the Schlieren image much closer to the porous structure because there is no problem with reflection resulting from taking the picture parallel to the porous structure (Figure 1). A distance of 1.3 mm is necessary because the retaining mechanism of the test sample blocks this area for the laser sheet.

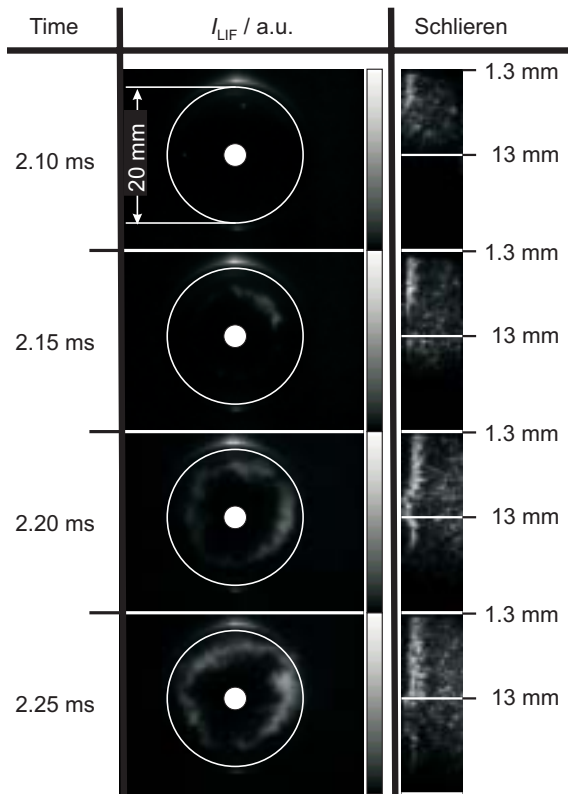


FIGURE 5 Simultaneous OH-LIF (yz-plane) and laser Schlieren (xy-plane) sequences using test sample No. 5. Direct flame transmission occurs.

Figure 5 visualizes rotation-symmetrically arranged OH radicals which are resulting from an evenly distributed direct flame transmission through the free annulus area of the test sample.

Additionally to the crimped ribbon flame arrester element Figure 6 shows the same kind of examination displayed in Figure 5 for a fiber structure with the specifications of test sample No. 9 that leads to an ignition on the hot surface (cp. Figure 4). According to Figure 4 the ignition in vessel 2 has to occur before the pressure in this vessel is rising. Therefore the ignition in vessel 2 occurs sometime between 10 ms and 15 ms after the ignition in vessel 1.

The examinations with the help of Schlieren technique and laser induced fluorescence of OH radicals are showing a hot gas flow including some OH radicals which result from the ignition in vessel 1 (Figure 6(a)).

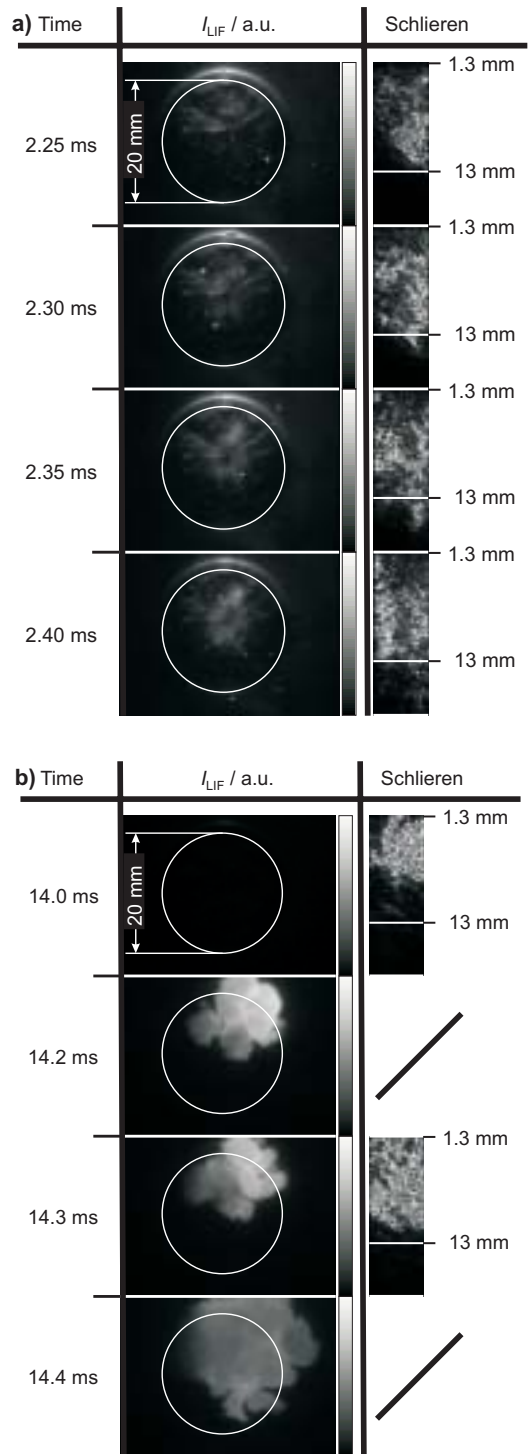


FIGURE 6 Simultaneous OH-LIF (yz-plane) and laser Schlieren (xy-plane) sequences using test sample No. 9. Ignition starts at the hot surface.

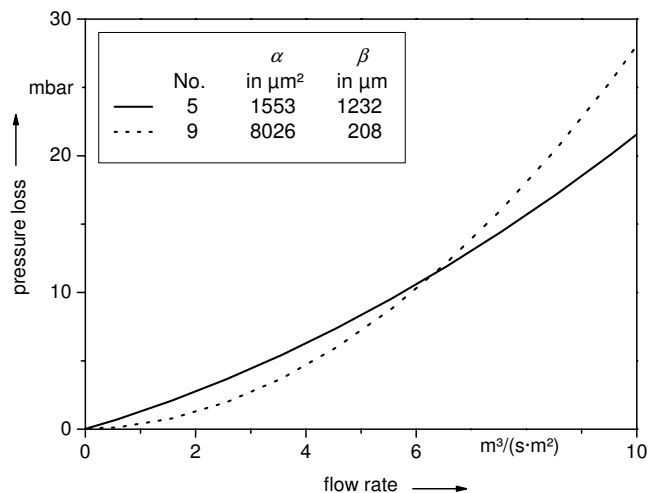


FIGURE 7  
Dependency between pressure loss and flow rate at 293 K and 1 bar for two different kinds of flame arrester elements.

No ignition in vessel 2 is visible in these sequences. The amplification used in Figure 6(a) is greater than in Figure 5. This is obvious because of the brighter looking reflections from the retaining ring although the reflections have the same intensity in every experiment.

14.0 ms after the ignition in vessel 1 Figure 6(b) shows the igniting process at the hot surface (the exact time of the ignition is not measurable, due to the local difference between the OH-LIF laser sheet and the hot surface, but this is not the point of interest though). The first Schlieren image in Figure 6(b) shows great differences in density resulting from the heating of the combustion. The OH-LIF picture shows no OH radicals because the flame front has not yet arrived at the laser sheet. In the following pictures combustion, visible through the great intensity of excited OH radicals, can be located. Figure 6(b) supports the theory of ignition on the hot surface because of the direction of the Schlieren propagation and its beginning directly beneath the test sample. It is important to be aware of the much lower amplification in Figure 6(b) than in Figure 5 and in Figure 6(a) noticeable in the invisibility of the reflections from the retaining ring.

Figure 7 shows the pressure losses calculated using Eq. (2) of two examined test samples (No. 5 and No. 9, Table 1) in dependency of the flow rate. The viscous

permeability coefficient  $\alpha$  and the inertia permeability coefficient  $\beta$  have been determined concerning ISO 4022 [2006]. The different developing of the pressure losses in Figure 7 are based on the different characteristics of the two flame arrester elements. The crimped ribbon geometry No. 5 consists of straight tubes (triangle-shaped) with smooth walls. That leads to a mostly laminar flow, consisting of a great inertia permeability coefficient  $\beta$  (Figure 7) (and therefore a small factor  $C$  in Eq. (2)), which induces a small pressure loss concerning to turbulences. So the linear part of Eq. (2) is dominant. In contrast the fibre structure No. 9 has only half the thickness of the crimped ribbon element and a greater porosity (cp. Table 1). Therefore the energy loss concerning to wall friction is much smaller than the one of the crimped ribbon with its narrow and relatively long tubes (great  $\alpha$  value cp. Figure 7 leads to a small factor  $B$  in Eq. (2)). Due to the tortuosity of the fibre structure the flow gets much more turbulent resulting in a small  $\beta$  value which makes the quadratic part of Eq. (2) getting dominant. This typical behaviour qualifies both types of flame arrester elements for different tasks. If the expected volume flows are relatively small, a flame arrester element with a high porosity is leading to a small pressure loss. But if the respected volume flows are greater a small tortuosity may be the better choice.

## CONCLUSIONS

With the determination of a safe gap value for porous structures used as flame arrester elements, we have introduced an easy to handle technical characteristic to quantify the property of such an element to avoid flame transmission (also cp. Mecke *et al.* [in press] and Mecke *et al.* [2007]). Additionally to the question of when a flame transmission occurs (in dependency of the initial pressure) we answered the question of how it is occurring. With the help of a Schlieren technique and laser induced fluorescence of OH radicals two different kinds of flame transmissions through flame arrester elements were observed. These are namely a direct flame transmission and an ignition at the hot surface of the porous structure, quite a long time after the explosion in vessel 1. In order to complete this work the flow resistances of fibre structure- and crimped ribbon elements were compared. Due to the different behaviour of the two kinds of flame arrester elements concerning their flow resistance it is reasonable to choose fibre structure elements when low volume flows are expected and crimped ribbon elements at high volume flows to generate a pressure loss as low as possible.

## ACKNOWLEDGEMENT

The authors would like to thank the German Federation of Industrial Cooperative Research Associations "Otto von Guericke e.V.", which has supported this work through the federal programs for innovation competence in medium-sized enterprises (PROINNO II), Grant KF 0043902LF4.

## NOMENCLATURE

$A$	area, $m^2$
$B$	factor in Eq. (2), $kg/(s \cdot m^4)$
$C$	factor in Eq. (2), $kg/m^7$
$d_f$	diameter of fibre, mm

$I_{LIF}$	intensity of OH-LIF, a.u. (arbitrary unit)
$l_f$	length of fibre, mm
$s$	thickness, m
$t_r$	thickness of ribbon, mm
$t_t$	thickness of test sample, mm
$\dot{V}$	volume flow, $m^3/s$
$w_g$	width of gap, mm
$\alpha$	viscous permeability coefficient, $m^2$
$\beta$	inertia permeability coefficient, m
$\varepsilon$	porosity, -
$\eta$	dynamic viscosity, $kg/(m \cdot s)$
$\tau$	wavelength, nm
$p$	pressure, $kg/(m \cdot s^2)$
$\rho_{solid}$	density of solid material, $kg/m^3$
$\rho_{porous\ structure}$	density of porous structure, $kg/m^3$

## REFERENCES

- Eckbreth, A. *Laser diagnostics for combustion temperature and species*. Overseas Publishers Association, Amsterdam, 1996.
- IEC 60079-1-1, *Electrical apparatus for explosive gas atmospheres – Part 1-1: Flameproof enclosures "d" - Method of test for ascertainment of maximum experimental safe gap*. International Electrotechnical Commission, 2002.
- ISO 4022, *Permeable sintered metal materials–Determination of fluid permeability*. International Organization for Standardisation, 2006.
- Mecke, S., Markus, D., Thedens, M., Engelmann, F., Hilliger, A. and Klausmeyer, U. Charakterisierung poröser Strukturen für den Einsatz in explosionsgeschützten elektrischen Geräten [Characterisation of porous structures for the application in explosion-proof electrical devices]. *Chemie Ingenieur Technik*, **79** (2007), 468–472.
- Mecke, S., Markus, D., Thedens, M., Engelmann, F., Hilliger, A. and Klausmeyer, U. (in press) Analysis of the flame quenching property of porous structures. *Proc. 5<sup>th</sup> International Seminar on Fire and Explosion Hazards*.
- Sadanandan, R., Markus, D., Schiessl, R., Maas, U., Olofsson, J., Seyfried, H., Richter, M. and Aldén, M. Experimental and numerical study of ignition by hot gas jets, *Proceedings of the Combustion Institute*, **31** (2007), 719–726.
- Schatt, W., Wieters, K. P. and Kieback, B. *Pulvermetallurgie [Powder metallurgy]*. Springer, Berlin, 2007.
- Steigert, S., Li, Z., Andersen, O., Stephani, G. and Schrooten, T. Intermetallic Fibre Materials for Hot Gas Filtration in Power Plants and Combustion Plants. *Proc. Materials Week 2000*, <[http://www.dgm.de/download/tg/523/523\\_0512.pdf](http://www.dgm.de/download/tg/523/523_0512.pdf)>.

Copyright of International Journal of Transport Phenomena is the property of Old City Publishing, Inc. and its content may not be copied or emailed to multiple sites or posted to a listserv without the copyright holder's express written permission. However, users may print, download, or email articles for individual use.